Available online at www.sciencedirect.com
ScienceDirect
Chinese Journal of Aeronautics 22(2009) 225-229
Chinese Journal of Aeronautics
www.elsevier.com/locate/cja

A High-speed Nature Laminar Flow Airfoil and Its Experimental Study in Wind Tunnel with Nonintrusive Measurement Technique

Zhu Jun*, Gao Zhenghong, Zhan Hao, Bai Junqiang

National Key Laboratory of Aerodynamic Design and Research, Northwestern Polytechnical University, Xi'an 710072, China

Received 7 May 2008; accepted 12 August 2008

Abstract

This article deals with an experimental study on the aerodynamic characteristics of a low-drag high-speed nature laminar flow (NLF) airfoil for business airplanes in the TST27 wind tunnel at Delft University of Technology, the Netherlands. In this experiment, in an attempt to reduce the errors of measurement and improve its accuracy in high-speed flight, some nonintrusive measurement techniques, such as the quantitative infrared thermography (IRT), the digital particle imaging velocimetry (PIV), and the shadowgraphy, are applied to obtain precise data about transition locations, separation on trailing edges, and lift/drag characteristics. The experimental results reveal that, in the high-speed flight, small angles of attack are helpful in retaining long laminar flows, preventing the vortex at the trailing edge from moving forward and thus imparting the airfoil and the high-lift and low-drag characteristics. The comparison of the measured results to the calculated ones proves the acceptability of the airfoil and its aerodynamic characteristics satisfying the design requirements.

Keywords: wind tunnels; particle imaging velocimetry; infrared thermography; shadowgraphy; high-speed nature laminar flow airfoil

1. Introduction

Business jet planes are gaining ever-increasing wide application in human travelling and commodity transportation. Not only that, but since the turn of 21st century, the price of fossil fuel has been soaring unabated. All these compel us to develop the low-drag laminar flow airfoils to attain the purpose of essentially enhancing the fuel efficiency[1].

After several years' effort, a high-speed nature laminar flow (NLF) airfoil was designed and manufactured. This article is meant to describe the experimental procedure of this airfoil in the TST27 wind tunnel at Delft University of Technology, the Netherlands. In the experiment, the transition location is measured with infrared thermography (IRT)[2-4] at different Mach numbers, Reynolds Numbers and angles of attack, the drag of the airfoil with particle imaging velocimetry (PIV)[5-7], the lift by integrating the pressure distribution, and the vortex on the trailing edge with shadowgraphy[8].

2. Airfoil Design and Experimental Methods

2.1. Airfoil design

Fig.1 shows the specially designed high-speed nature laminar flow airfoil together with the baseline airfoil of NLF-0213 known as the low-speed nature laminar flow airfoil, where C means the chord length of airfoil.

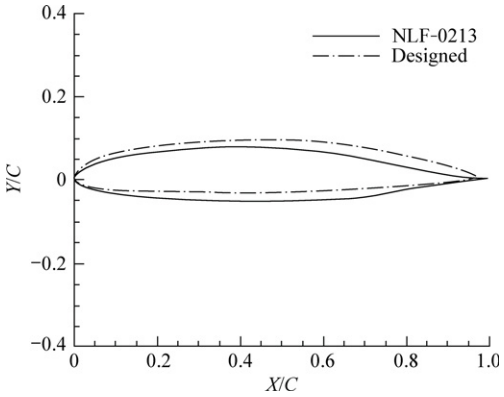

Fig.1 Comparison of airfoils.

In order to retain a long laminar flow on the surface of the airfoil within a broad range of angles of attack,

*Correponding author. Tel: +86-13636806896.
E-mail address: solomonzj@sina.com

doi: 10.1016/S1000-9361(08)60091-6

the separation ramp concept[9-11] that was first proposed by F. X. Wortmann at high Reynolds numbers in high-speed flight is introduced.

This design used the inverse method under the preset following conditions: Ma_∞=0.69, Re=2.85×10^6. Fig.2 shows the pressure distribution of NLF-0213 in this state. In addition, to realize the separation, the ramp pressure coefficient C_p distribution at the rear part of the upper surface takes the special shape of pressure recovery.

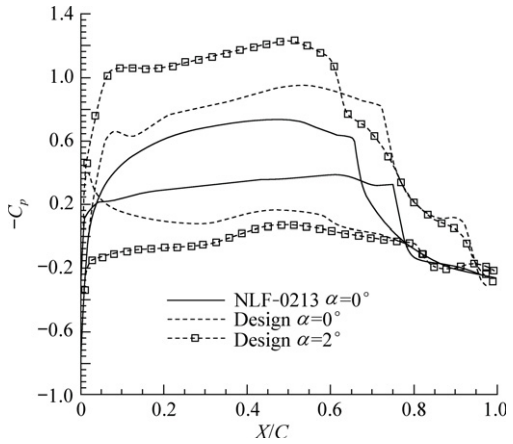

Fig.2 Comparison of pressure distributions.

The aerodynamic characteristics of the airfoil are calculated with Navier-Stokes equations. The turbulent model is shear stress transport (SST) k-ω two-equation model with γ-θ transition model.

From Fig.3, as the result of the separation ramp, a stable separated vortex turns up in the vicinity of the trailing edge. Fig.2 displays the pressure distribution of the designed airfoil at angle of attack $\alpha = 0°$ and $\alpha = 2°$. It demonstrates that a longer favorable pressure gradient would stay on the upper surface.

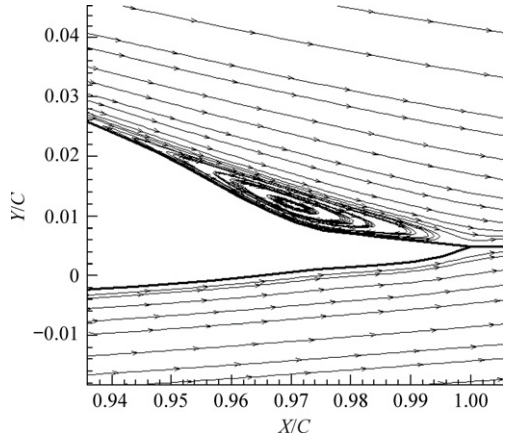

Fig.3 Streamline votex.

From the calculation, it follows that when the angle of attack increases, the special shape of pressure recovery would not change. As a result, the stalling angle remains unchanged and the maximal lift coefficient C_L reaches 0.9. At the same time, the special shape of pressure recovery will be helpful to maintain a longer favorable pressure gradient on the upper surface and retain the longer laminar flow on the upper surface within a broad range of angles of attack and thus maintaining a low drag. Compared with the traditional nature laminar flow airfoil, this proposed airfoil is characterized by high-lift and low-drag aerodynamic properties.

2.2. Experimental methods

It seems difficult to make accurate determination of drags and transition locations of an airfoil, especially of a nature laminar flow airfoil, in a wind tunnel. With traditional methods, a wake rake would be put in the flow field to measure the drag, which might disturb the field and increase the errors of measurement. In the case of using oil flow technique to find transition locations, it is important yet difficult to control the thickness of oil and eliminate the effects of it.

The usage of any traditional measurement methods inclusive of the above mentioned in wind tunnel should not steer clear of the problems that the flow fields must be affected; some nonintrusive methods, such as IRT, PIV, and shadowgraphy were invented.

As a convenient way to measure the surface temperature of an object, IRT is superior to other methods in, just name a few, its nonintrusion and removal of need for installing instruments on the model or in the flow path. Because the laminar flow has a different wall temperature response from the turbulent flow, the transition can be detected by the IRT.

As a nonintrusive technique, PIV is used to measure an instantaneous moderate flow velocity on a single plane of interest. By introducing a pulsed laser sheet into the flow, PIV records the motion of particles in the plane, making the instantaneous spatial structure of the two component velocity fields visible. Thus, from the velocity field, the drag can be determined.

In this experiment, the drag coefficient C_D is computed from the velocity. A velocity profile in the wake is used to make an estimate of the momentum deficit and therefore an estimate of the force exerting on the airfoil. At the same time, the compressibility effects are taken into account in the high subsonic state where the measurements are carried out.

Shadowgraphy is an optical technique that yields a qualitative representation of the spatial distribution of density variations in the flow field. It is more suitable to detect shear layers and turbulent structures.

In shadowgraphy, because the density varies in the flow field, the light rays are deflected so as to cause intensity changing in the image. In practice, the bright spots in the image mean where light rays have converged and dark spots where light rays have diverged. Taking a shock wave image as an example, the light region is observed to be followed by a dark region enabling the separation, and, in turn, a possible transition in the boundary layer can be easily discovered visually.

3. Experimental Facilities

The TST27 is a transonic/supersonic blow down wind tunnel of which Mach number ranges from 0.5 to 4.2. Composed of modular parts, the wind tunnel has a test section with a width of 280 mm and an adjustable height of 250 mm to 270 mm as a function of the Mach number.

The infrared measurements were carried out using an Agema 880 long wave band (LWB) camera. For the camera to be able to acquire a picture of the model, a germanium window has been installed in the test section of the wind tunnel.

During measurement, a double-pulsed Nd: yttrium aluminum garnet (YAG) laser producing a wave length of 532 nm is employed as the illumination source. The tracer particles are distributed by a seed rake placed in the seed chamber. The particles have a mean diameter of 1 μm. The seed generator is essentially a Laskin nozzle, which creates small particles of di-ethyl hexyl sebacate (DEHS). An impacted plate is used to discard the large oil droplets. Fig.4 shows the scheme of the PIV setup installed in the TST27 wind tunnel.

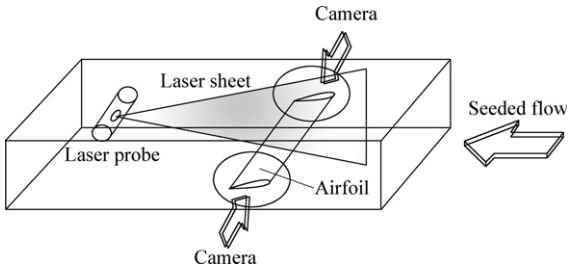

Fig.4 Schematic of PIV setup.

A xenon spark (50 μs flask) light has been synchronized using a charge-coupled device (CCD) camera. The system is capable of producing five images per second.

This airfoil has a chord length of 100 mm and a span of 280 mm, which corresponds to the horizontal span of the test section of TST27 transonic/supersonic wind tunnel. In this model, 35 pressure ports are arranged that are used to measure pressure.

4. Results

This article has performed an experiment to determine the aerodynamic characteristics of this airfoil including lift, drag, and separation transition.

4.1. Lift measurement

Pressure taps were used to determine the static pressure on the surface of the airfoil and a wake rake and the total pressure in the wake. Fig.5 shows the C_L-α curve, which is acquired by numerically integrating the pressure distribution over the airfoil surface. From it, it is clear that the largest C_L is about 0.9, which meets the high-lift design demands. The difference between the calculated and the experimental results, which might stem from insufficient pressure ports considered in integration, is too small that can be ignored.

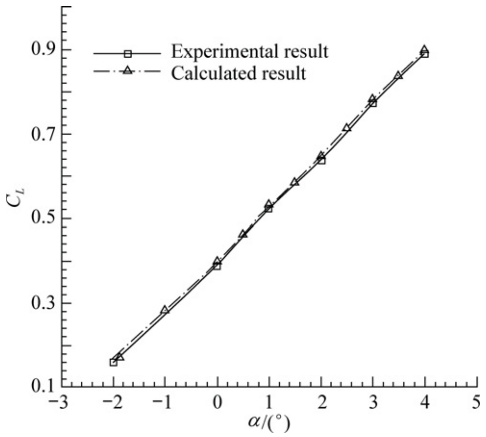

Fig.5 Lift coefficients at different angles of attack.

4.2. Drag measurement

Fig.6 shows the averaged flow velocity vector of $\alpha = 0°$, from the PIV measurement, and Fig.7 shows the instantaneous flow velocity vector of $\alpha = 4°$, at $Ma_\infty = 0.69$, $Re = 2.85\times10^6$.

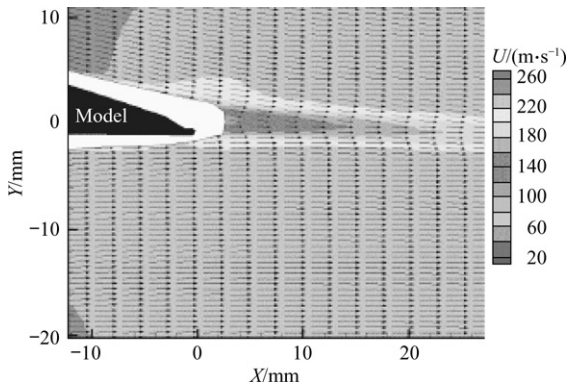

Fig.6 Averaged flow velocity vector ($\alpha = 0°$).

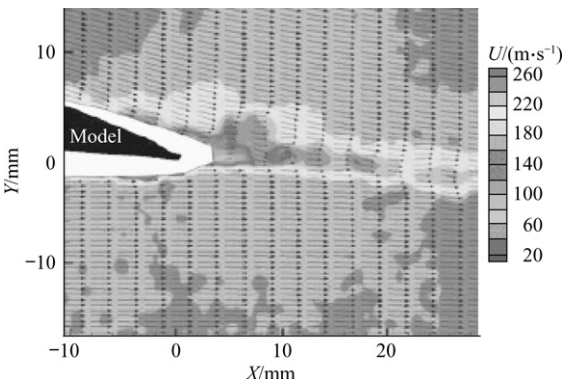

Fig.7 Instantaneous flow velocity vector ($\alpha = 4°$).

Fig.8 shows the drag coefficient polar of the airfoil obtained from the wake pressure and the PIV wake velocity profile at $Ma_\infty = 0.69$, $Re = 2.85\times10^6$, and different α. The airfoil satisfies the low-drag design demands.

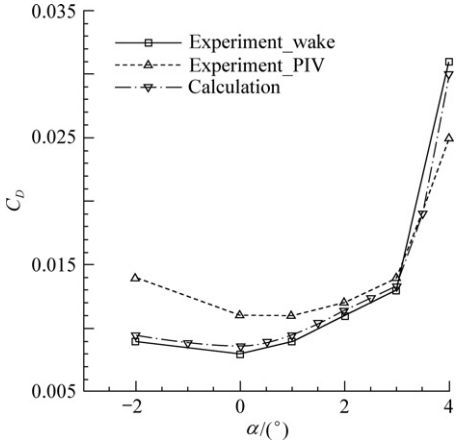

Fig.8 Comparison of drag coefficients at different α.

From Fig.8, it is observed that large differences exist between the drag coefficients acquired by using wake rake data and by PIV data at some large angles of attack. This might be ascribed to the relatively thick wake of this airfoil not fully captured into the field of view during the PIV measurements. The wake is large and therefore the height of the field of view chosen is not sufficient to cover the full extent of the velocity deficit. However, this problem is not encountered by the wake rake, which traverses a larger height and is therefore able to cover the entire velocity deficit. There are some differences between calculated and experimental results near $\alpha = 0°$ because the viscous drag is assumed small in calculation.

4.3. Transition location measurement

Fig.9 shows the heat flux from infrared (IR) camera on the upper surface at $Ma_\infty = 0.69$, $Re = 2.85\times10^6$, and $\alpha = -1°$. In Fig.10, the nondimensional heat transfer curve shows the transition location of about 67%.

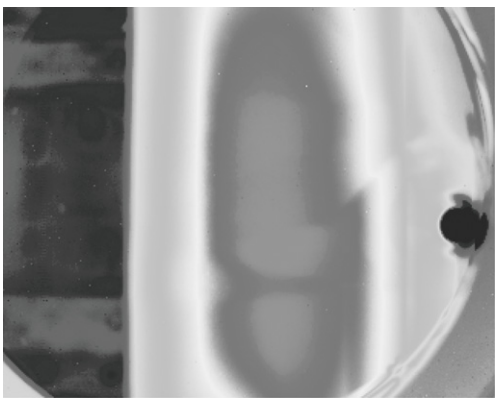

Fig.9 Heat flux from IR camera.

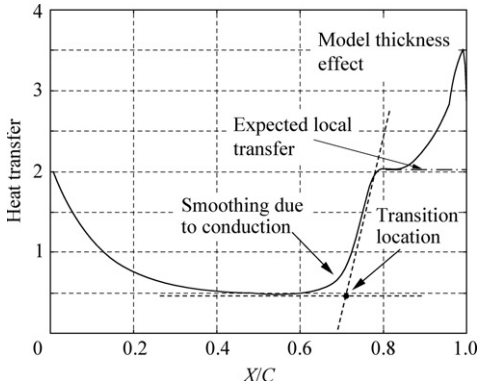

Fig.10 Nondimensional heat transfer.

Table 1 lists the transition locations from IRT and calculation at other angles of attack. When the angles of attack are less than 2°, a longer laminar flow stays on the upper surface of the airfoil. At the same time, by comparison with the transition locations obtained from IRT and from calculation evidence, it can be observed that the results from the wind tunnel are reasonably acceptable.

Table 1 Comparison of transition locations

α /(°)	Transfer location	
	IRT	Calculation
–2	65.0	61
–1	67.0	64
0	67.5	66
2	53.5	50
4	22.0	17

4.4. Vortex measurement

From Fig.6 with PIV at $\alpha = 0°$, a stable wake vortex can be seen on the trailing edge of the airfoil, but from Fig.7, it becomes unstable. When α reaches 4°, a large separation area turns up on the upper-surface of the airfoil.

The shadowgraphy measurements on the airfoil are performed in order to observe density gradients and, in particular, identify the presence of separated shear layers. From Figs.11-12, it is known that the vortex on

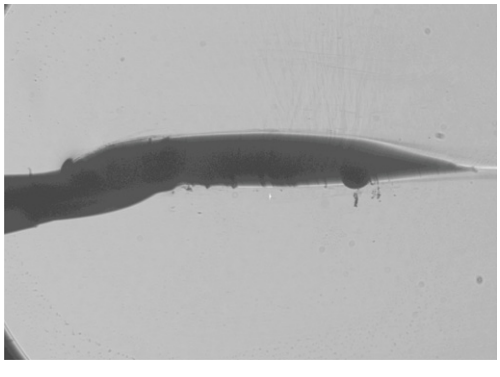

Fig.11 Averaged shadowgraphy of flow field ($\alpha = 0°$, $Ma_\infty = 0.69$).

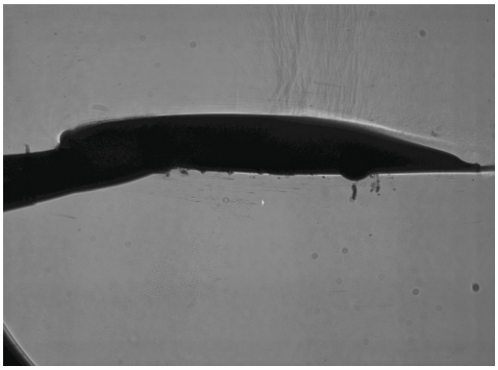

Fig.12 Averaged shadowgraphy of flow field ($\alpha = 3°$, $Ma_\infty = 0.69$).

the trailing edge of the airfoil remains unchanged without moving forward as the angle of attack varies.

5. Conclusions

The experimental and measured results have evidenced that the high-speed nature laminar flow airfoil is triumphantly designed and manufactured. From $\alpha = -2°$ to $\alpha = 2°$, it is in possession of a long laminar flow on the upper surface and a stable separated vortex on the trailing edge. Thus, it is characterized by the high-lift and low-drag properties in high-speed flight. Therefore, the aerodynamic characteristics of the airfoil satisfy the design demands.

References

[1] Fujino M, Yoshizaki Y, Kawamura Y. Natural-laminar-flow airfoil development for a ligntweight business jet. Journal of Aircraft 2003; 40(4): 609-615.

[2] McCafferty D J, Moncrieff J B, Taylor I R, et al. The use of IRT to measure the radiative temperature and heat loss of a barn owl (tyto alba). Jounal of Thermal Biology 1998; 23: 311-318.

[3] Ovechkin A M. Application of IRT in diagnostics of acute viral infections of respiratory system. Medical Thermography 2002; 1(2): 70-76.

[4] Le Saint Y, Marchand M, Millan P, et al. An overview of infrared thermography techniques used in large wind tunnels. Aerospace Science and Technology 2002; 6(5): 355-366.

[5] Adrian R J, Prasad A K. Stereoscopic particle image velocimetry applied to liquid flows. Sixth International Symposium on Applications of Laser Techniques to Fluid Mechanics, 1992; 91-108.

[6] Tedeschi G, Gouin H, Elena M. Motion of tracer particles in supersonic flows. Experiments in Fluids 1999; 26(4): 288-296.

[7] Scarano F. Iterative image deformation methods in PIV. Measurement, Science and Technology 2002; 13: R1-R19.

[8] Aso S, Maekawa S, Okuyama S. Intense studies on unsteady secondary separations and oscillating shock waves in three-dimensional shock waves/turbulent boundary layer interaction regions induced by sharp and blunt fins. AIAA-93-2939, 1993.

[9] Mark D. Design and experiment results for a high-attitude, long-endurance airfoil. Journal of Aircraft 1989; 26(2): 148-153.

[10] Shiokawa M, Matsushima K, Nakahashi K. Design and aerodynamics of lift enhancement control for a single element airfoil. AIAA-2005-853, 2005.

[11] Patel M P, Ng T T, Vasudevan S. Plasma actuators for hingeless aerodynamic control of an unmanned air vehicle. AIAA-2006-3495, 2006.

Biography:

Zhu Jun Born in 1979, he received M.S. from Northwestern Polytechnical University in 2003, and now is a Ph.D. candidate in the same school. His research interest lies in flight vehicle design.
E-mail: solomonzj@sina.com